LETTER

doi:10.1038/nature22030

Large historical growth in global terrestrial gross primary production

J. E. Campbell[1], J. A. Berry[2], U. Seibt[3], S. J. Smith[4], S. A. Montzka[5], T. Launois[6]†, S. Belviso[6], L. Bopp[6]† & M. Laine[7]

Growth in terrestrial gross primary production (GPP)—the amount of carbon dioxide that is 'fixed' into organic material through the photosynthesis of land plants—may provide a negative feedback for climate change[1,2]. It remains uncertain, however, to what extent biogeochemical processes can suppress global GPP growth[3]. As a consequence, modelling estimates of terrestrial carbon storage, and of feedbacks between the carbon cycle and climate, remain poorly constrained[4]. Here we present a global, measurement-based estimate of GPP growth during the twentieth century that is based on long-term atmospheric carbonyl sulfide (COS) records, derived from ice-core, firn and ambient air samples[5]. We interpret these records using a model that simulates changes in COS concentration according to changes in its sources and sinks—including a large sink that is related to GPP. We find that the observation-based COS record is most consistent with simulations of climate and the carbon cycle that assume large GPP growth during the twentieth century (31% ± 5% growth; mean ± 95% confidence interval). Although this COS analysis does not directly constrain models of future GPP growth, it does provide a global-scale benchmark for historical carbon-cycle simulations.

Climate change can be accelerated or dampened by feedbacks with terrestrial ecosystems[6]. The largest and most uncertain of these ecosystem feedbacks is enhanced photosynthetic CO_2 uptake resulting from increasing atmospheric CO_2 levels[4]. Clear evidence has been obtained from archived leaf material that increasing CO_2 levels do increase photosynthetic metabolism, and much has been learnt about this feedback and about other influences on photosynthesis (for example, nitrogen deposition) from short-term and small-scale studies[1,3,7]. However, we lack global-scale, measurement-based estimates of the historical growth in photosynthetic CO_2 uptake (that is, growth in GPP). This knowledge gap leads to a wide spread of GPP growth estimates from different carbon/climate models, ranging from +5% to +34% over the past century, and from +10% to +52% over the next century[3].

Here we seek to address this knowledge gap by using COS measurements to estimate historical growth of global GPP. This approach is based on the knowledge that the dominant global sink of atmospheric COS is uptake by terrestrial plant leaves, through a process that is related to photosynthesis[8–11]. While other terrestrial ecosystem fluxes can be substantial at times[12–14], the COS plant sink appears to be dominant at annual and continental scales[15–17]. The plant COS uptake is primarily compensated by ocean, industrial, and biomass burning sources[18–21]. Without compensating changes in other sources or sinks, a change in plant uptake, and hence in GPP, would result in a new balance point in COS concentration with a relaxation time of about two years. This is the basis for our present analysis.

Our analysis focuses on the long-term record of atmospheric COS concentrations from Antarctica (Fig. 1a)[5,22], which is a good proxy for the total atmospheric burden of COS. The Antarctic record—derived from measurements of air trapped in Antarctic ice and firn (granular snow deposited in previous years), and from ambient air samples—is consistent with independent long-term data from ground-based infrared solar spectra and global flask sampling (Fig. 1b)[23–25]. The Antarctic record shows stability of COS concentrations in the preindustrial era, indicating that the natural sources and sinks were relatively stable over this time. However, the industrial period shows an increase in COS levels (Fig. 1a) that is unprecedented in the 54,300-year COS record. This increase in Antarctic COS concentrations in the industrial period is clear evidence of a global industrial source[5]. In a separate study, we used economic data to construct the history of COS industrial sources[18]. While the magnitude of the industrial source is uncertain (Fig. 2a), the relative change in the industrial source in time is well constrained by economic data (Fig. 2b)[18].

In addition to the industrial source, we also consider here the potential for other global sources and sinks to explain the trends in the Antarctic COS record. We analyse a wide range of source and sink estimates, including plant COS uptake linked to GPP (Fig. 2c, d), with GPP growth obtained from 11 different global carbon/climate models[3]. With these data sets in hand, we seek to identify the most plausible combination of source and sink simulations that explain the Antarctic COS record.

These simulations are based on a Monte Carlo, two-box, global modelling approach. The model outputs are historical time series of atmospheric COS mixing ratios ([COS]) for the years 1900 through to 2013, which we compare to the Antarctic COS record. The model inputs are time-series estimates of global sources and sinks, which are a function of their magnitude scalars (F) and normalized time-trend vectors ($\boldsymbol{\Phi}$) as follows:

$$\frac{\mathrm{d}[\mathrm{COS}]}{\mathrm{d}t} = F_{\mathrm{AN}}\boldsymbol{\Phi}_{\mathrm{AN}} + F_{\mathrm{BB}}\boldsymbol{\Phi}_{\mathrm{BB}} + F_{\mathrm{OC}}\boldsymbol{\Phi}_{\mathrm{OC}} + F_{\mathrm{SS}}\boldsymbol{\Phi}_{\mathrm{SS}} - F_{\mathrm{P}}\boldsymbol{\Phi}_{\mathrm{P}}[\mathrm{COS}] - F_{I}\boldsymbol{\Phi}_{I}[\mathrm{COS}] - F_{\mathrm{S}}\boldsymbol{\Phi}_{\mathrm{S}}[\mathrm{COS}] + \frac{1}{\tau}\Delta[\mathrm{COS}] \quad (1)$$

including sources from industry (AN, anthropogenic), biomass burning (BB), oceans (OC), and soils (SS), and sinks from terrestrial plants (P), atmospheric oxidation (I), and soils (S), and a transport rate (τ) scaled by the inter-hemispheric gradient (Δ[COS]). The sources include direct emissions as well as indirect sources from emissions of short-lived precursors that are rapidly oxidized to COS in the atmosphere. Other sources and sinks may be important locally but were not included in our analysis because of their small contributions to global budgets.

The plant uptake was further divided into parameters for GPP (F_{GPP}, $\boldsymbol{\Phi}_{\mathrm{GPP}}$) and the normalized ratio of plant COS uptake to GPP (F_{LRU}, $\boldsymbol{\Phi}_{\mathrm{LRU}}$, where LRU is leaf-scale relative uptake). For the normalized ratio

[1]Sierra Nevada Research Institute, University of California, Merced, California 95343, USA. [2]Department of Global Ecology, Carnegie Institution for Science, Stanford, California 94305, USA. [3]Department of Atmospheric and Oceanic Sciences, University of California, Los Angeles, California 90095, USA. [4]Joint Global Change Research Institute, Pacific Northwest National Laboratory, College Park, Maryland 20740, USA. [5]Earth System Research Laboratory, National Oceanic and Atmospheric Administration, Boulder, Colorado 80305, USA. [6]Laboratoire des Sciences du Climat et de l'Environnement, IPSL, CNRS/CEA/UVSQ, 91191 Gif sur Yvette, France. [7]Finnish Meteorological Institute, Helsinki 00560, Finland. †Present address: INRA, UMR 1391 ISPA, 33140 Villenave d'Ornon, France (T.L.); Laboratoire de Météorologie Dynamique, IPSL, CNRS/ENS/UMPC/X, 75005 Paris, France (L.B.).

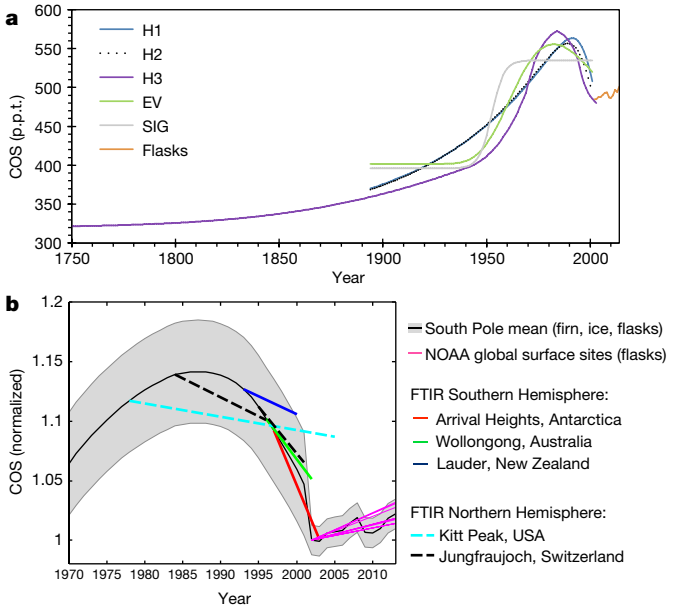

Figure 1 | Measurement-based histories of atmospheric COS at South Pole and global sites. a, Alternative histories that are consistent to varying degrees with measurements of COS at the South Pole from air trapped in Antarctic ice and firn, and from ambient air[5]. See Supplementary Information for further information on these histories. The 'flasks' line (orange) shows the annual mixing ratio for ambient air collected at the South Pole[9]. p.p.t., parts per 10^{12}. **b**, Normalized mixing ratios of COS from South Pole atmospheric firn histories, global surface flasks, and Fourier transform infrared spectroscopy (FTIR)-based solar observations[23–25]. For the five firn-based histories, the mean (black solid line) and standard deviation (grey shading) are plotted. Global surface flask observations (thin pink lines, one for each site) were obtained from the NOAA monitoring network (sited at Barrow, Alaska; Mauna Loa, Hawaii, USA; Niwot Ridge, Colorado, USA; Alert, Canada; Cape Kumukahi, Hawaii, USA; Mace Head, Ireland; Cape Grim, Australia; and Tutuila, American Samoa).

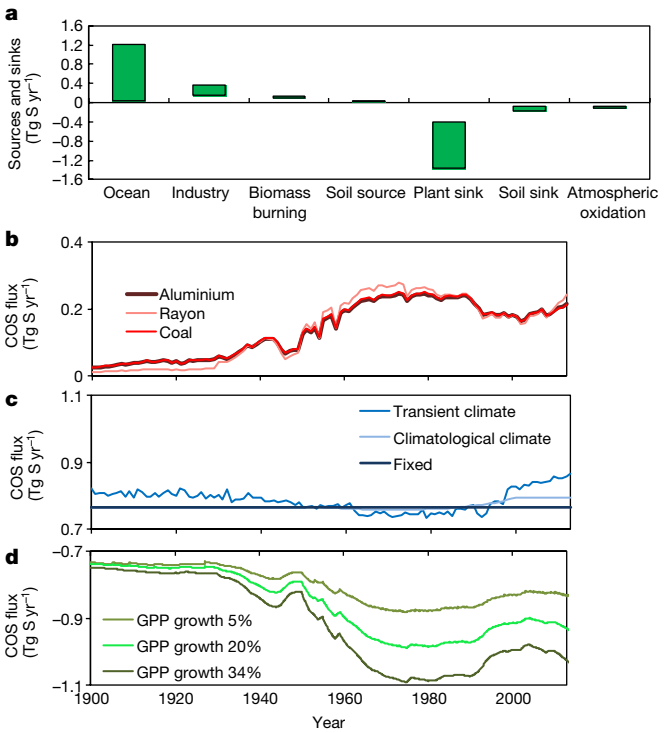

Figure 2 | *A priori* distribution of present-day magnitudes and alternative time trends for components of the global COS budget. **a**, Present-day (2013) magnitudes for the dominant components of the global COS budget. The widths of the bars show the uncertainties. We used these 2013 budget distributions to estimate magnitude scalar parameters (*F* values, used in **b–d**) using Equation (1). The ranges shown are taken from the literature, and are the best estimates for the ocean, and the minimum and maximum values for the other components (see Supplementary Information Sections 3 and 4). **b–d**, Alternative scenarios representing the range of plausible time trends in COS flux resulting from industrial sources (**b**), ocean sources (**c**), and plant uptake (**d**). Time trends for the smaller budget components (biomass burning, soils, and atmospheric oxidation) were also included in our model and are shown in Supplementary Information. Our Monte Carlo simulations randomly drew from *a priori* distributions to simulate the history of COS mixing ratios. The three industrial time trends (**b**) represent extreme cases that result from maximizing the contributions from the rayon, aluminium or coal sectors. The three ocean trends (**c**) were a fixed scenario with no trend, an ocean simulation driven by climatological forcing, and an ocean simulation driven by temporally explicit climate forcing. The plant-uptake trends (**d**) are from simulations driven by a range of historical GPP growth rates (5%, 20% or 34%). See Supplementary Information for further details.

of COS plant uptake to GPP (LRU), we considered both empirical and mechanistic models (see Supplementary Information section 4.1). GPP histories were either based on linear relationships to atmospheric CO_2 levels, or obtained from 11 global carbon/climate models. We also used recent data-driven estimates of present-day global GPP as an input for the COS simulations[26,27].

We explored the range of possible simulations using a Monte Carlo approach. In each Monte Carlo simulation, a set of *F* and $\boldsymbol{\Phi}$ values was selected at random from uniform distributions of *a priori* values on the basis of a review of the recent literature. We evaluated the agreement between the Monte Carlo simulation output and the Antarctic record using the root mean squared (r.m.s.) error.

We found that the r.m.s. error of the Monte Carlo simulations (Supplementary Fig. 11) was most sensitive to three input variables: ocean COS magnitude (F_{OC}), anthropogenic COS magnitude (F_{AN}) and the GPP time trend ($\boldsymbol{\Phi}_{GPP}$). Given the high sensitivity of these three variables, we explored optimization scenarios that adjust these three input variables in order to minimize the r.m.s. error of the model output. We also considered optimization scenarios in which all input variables were adjusted to minimize the r.m.s. error (Supplementary Information Fig. 7).

Our first Monte Carlo simulations minimized the r.m.s. error by adjusting the ocean magnitude scalar (F_{OC}) to best match the Antarctic record while randomly drawing from the *a priori* distributions for all other input variables (Fig. 3a). These Monte Carlo simulations provided a poor fit to the Antarctic record (Fig. 3a).

Next we explored the influence of the other two highly sensitive variables (F_{AN} and $\boldsymbol{\Phi}_{GPP}$). We considered simulations in which the ocean magnitude was optimized while the anthropogenic magnitude and GPP time trend were specified. When the GPP time trend was specified for low GPP growth, the r.m.s. error remained high (Fig. 3b). However, when the GPP trend was specified for high GPP growth, the simulations were able to capture the trends relatively well when combined with a large industrial COS magnitude (Fig. 3c, blue line).

To account for interactions between input variables, we performed another set of Monte Carlo simulations in which these three sensitive input variables were simultaneously optimized (Fig. 3d). While this set of simulations underestimated the peak COS mixing ratios in the 1980s, it did result in a 50% reduction in r.m.s. error (a 46% reduction in mean bias) relative to the simulations that optimized F_{OC} only. The optimal value of GPP growth from these simulations was 31% ± 5% (mean ± 95% confidence interval), which is at the high end of the historical range of +5% to +34% used in global carbon/climate models, providing a new global estimate of this largely unconstrained process.

For these simulations we used the mean Antarctic record, but we also repeated the analysis with individual Antarctic records (H1, H2,

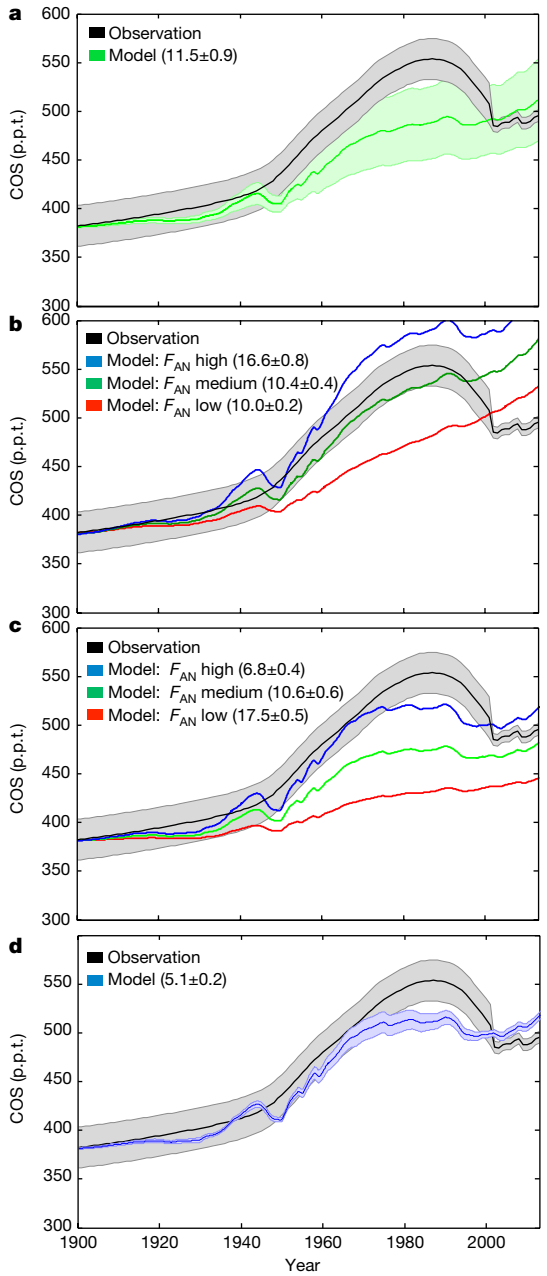

Figure 3 | Long-term trends in global atmospheric COS concentrations. The observed Antarctic records of COS concentrations (black lines) represent the mean of five firn-based histories and ambient measurements from 1900 to 2013 (ref. 5). Also shown are COS concentrations that emerge from Monte Carlo optimization simulation models; optimization minimizes the model r.m.s. mixing ratio error with respect to the difference between the modelled and the observed time series from 1900 to 2013. (The r.m.s. errors are listed in each panel as the mean COS concentration ± 95% confidence interval.) **a**, In 'optimize F_{OC}' simulations, the ocean magnitude scalar (F_{OC}) is optimized while all other variables are drawn at random from *a priori* distributions. **b**, In 'minimum GPP growth' simulations, F_{OC} is optimized; the GPP time trend (Φ_{GPP}) is set to the minimum *a priori* history (5% growth); the industrial magnitude (F_{AN}) is specified (see figure); and all other parameters were randomly drawn from *a priori* distributions. **c**, The 'maximum GPP growth' simulations are equivalent to those in **b**, except that Φ_{GPP} is set to the maximum *a priori* growth history (34% growth). **d**, Additional simulations optimize F_{OC}, F_{AN} and Φ_{GPP}, while making random draws from *a priori* distributions for all other parameters. Model uncertainty (green/blue shaded areas) accounts for uncertainty in the non-optimized source and sink parameters (standard deviation; $n = 100$). Observation uncertainty (grey shaded areas) accounts for the standard deviation between the five firn-based histories and measurement uncertainty.

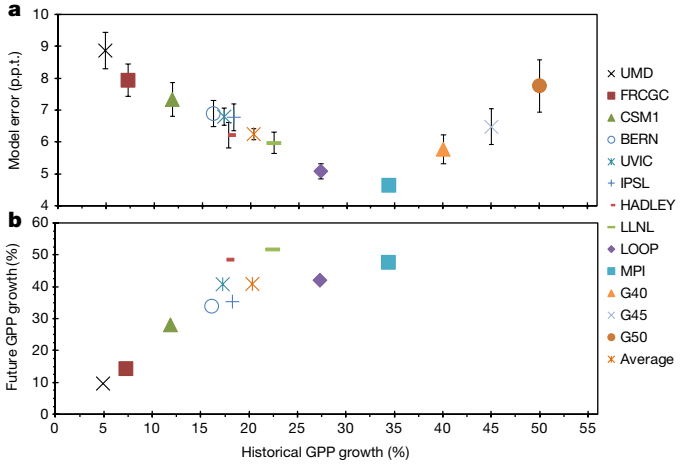

Figure 4 | Comparison of carbon/climate models. a, Atmospheric COS model errors obtained using a range of GPP histories. Percentage increases in GPP growth over the twentieth century were taken from published carbon/climate models (as shown at the right); in addition, we added three hypothetical scenarios with more extreme GPP growth (40%, 45% or 50%, in scenarios G40, G45 and G50, respectively). Each GPP history was used as an input for a different set of Monte Carlo atmospheric COS simulations. The r.m.s. error for each set of COS simulations was calculated by using the difference between the simulated COS mixing ratios and the observed atmospheric COS mixing ratios (as derived from Antarctic ice-core, firn-air, and ambient flask samples) for the years 1900 to 2013 (ref. 5). The simulations optimized two variables (magnitude scalars for ocean and anthropogenic COS sources), and obtained estimates of all other parameters through random draws from their *a priori* distributions. The error bars represent standard deviations for each set of Monte Carlo simulations ($n = 100$). **b**, For each carbon/climate model, historical GPP growth (resulting from simulations for the twentieth century) is plotted against projected future GPP growth (resulting from simulations for the twenty-first century).

H3, EV and SIG from Fig. 1). Optimization simulations based on each individual Antarctic record gave similarly high optimal GPP growth results (95% confidence intervals range from 22% to 34% GPP growth).

Although the preceding simulations used an *a priori* range of GPP time trends (Φ_{GPP}) that were modelled as a linear function of atmospheric CO_2, we also tested GPP histories obtained from carbon/climate models (Fig. 4). All COS simulations using these GPP histories resulted in reductions in r.m.s. error relative to COS simulations that had no historical growth in GPP. Some GPP growth scenarios performed much better than others. The lowest r.m.s. error was achieved with COS simulations that used GPP from carbon/climate models with the highest historical GPP growth rates (25% to 35% growth).

The simulations described so for had a range of GPP magnitudes (F_{GPP}) of 107–152 Pg C yr^{-1}, which we obtained from carbon/climate models. However, measurement-based estimates of GPP are as large as 175 Pg C yr^{-1} (refs 26, 27). After expanding our GPP range to include these higher estimates, we found a negligible effect on our optimal estimate of GPP growth (a change in r.m.s. error of less than 1%, and optimal GPP growth).

In carbon/climate models, GPP growth over the twentieth century correlates with GPP growth predicted over the twenty-first century (Fig. 4b). For example, the University of Maryland (UMD) carbon/climate model has the lowest GPP growth rate over the twentieth century, and it also simulates the lowest GPP growth rate over the twenty-first century. While this close relationship suggests that historical GPP analysis is relevant to projections, the relationship may be weakened in next-generation models that include more-restrictive nutrient parameterizations.

Our analysis is based on a global-scale constraint. Previously published estimates of GPP trends are not directly comparable with our

results, because such estimates were generally obtained from studies of smaller spatial and shorter temporal scales. Furthermore, previous evidence is mixed with respect to whether GPP growth is small or large. Plot-scale measurements from free-air CO_2 enrichment (FACE) experiments have had equivocal results, which is probably because of the very limited number of experiments relative to the large spatial heterogeneity and long period for global GPP growth[1,3]. Of the two decadal-scale forest FACE experiments, one found an initial 23% GPP growth that declined over time to 9% owing to nutrient limitation, while the other found a range of 22% to 30% GPP growth that was sustained. Observation-based estimates of present global GPP also vary widely and are not yet useful for estimating temporal trends[26,27]. Long-term trends in satellite vegetation indices from the year 1982 show positive trends in greenness, but are more directly related to plant structure than to GPP growth[28,29]. Change in background atmospheric CO_2 mixing ratios relative to fossil-fuel emissions have been attributed to GPP growth, but the combined influence of photosynthesis and respiration makes it difficult to constrain GPP with CO_2 data alone[30]. Analysis of historical growth in the seasonal atmospheric CO_2 amplitude supports substantial GPP growth[31,32], but again cannot be directly compared with our work because these amplitude observations are confined to Northern Hemisphere high latitudes.

Our COS analysis provides evidence of increases in historical GPP of $31\% \pm 5\%$ over the twentieth century at the global scale. The range of growth rates found here provides a major new constraint for evaluating historical simulations of Earth system models, such as in fusion frameworks that combine multiple observations[33].

Data Availability The authors declare that data supporting the findings of this study are available within the paper and its Supplementary Information files. All other data are available from the corresponding author upon reasonable request.

Received 10 January 2012; accepted 23 February 2017.

1. Norby, R. J., Warren, J. M., Iversen, C. M., Medlyn, B. E. & McMurtrie, R. E. CO_2 enhancement of forest productivity constrained by limited nitrogen availability. *Proc. Natl Acad. Sci. USA* **107,** 19368–19373 (2010).
2. Schimel, D., Stephens, B. B. & Fisher, J. B. Effect of increasing CO_2 on the terrestrial carbon cycle. *Proc. Natl Acad. Sci. USA* **112,** 436–441 (2015).
3. Friedlingstein, P. *et al.* Uncertainties in CMIP5 climate projections due to carbon cycle feedbacks. *J. Clim.* **27,** 511–526 (2014).
4. Arneth, A. *et al.* Terrestrial biogeochemical feedbacks in the climate system. *Nat. Geosci.* **3,** 525–532 (2010).
5. Montzka, S. A. *et al.* A 350-year atmospheric history for carbonyl sulfide inferred from Antarctic firn air and air trapped in ice. *J. Geophys. Res.* **109,** D22302 (2004).
6. Field, C. B., Lobell, D. B., Peters, H. A. & Chiariello, N. R. Feedbacks of terrestrial ecosystems to climate change. *Annu. Rev. Environ. Resour.* **32,** 1–29 (2007).
7. Ehlers, I. *et al.* Detecting long-term metabolic shifts using isotopomers: CO_2-driven suppression of photorespiration in C3 plants over the 20th century. *Proc. Natl Acad. Sci. USA* **112,** 15585–15590 (2015).
8. Sandoval-Soto, L. *et al.* Global uptake of carbonyl sulfide (COS) by terrestrial vegetation: estimates corrected by deposition velocities normalized to the uptake of carbon dioxide (CO_2). *Biogeosciences* **2,** 125–132 (2005).
9. Stimler, K., Montzka, S. A., Berry, J. A., Rudich, Y. & Yakir, D. Relationships between carbonyl sulfide (COS) and CO_2 during leaf gas exchange. *New Phytol.* **186,** 869–878 (2010).
10. Wohlfahrt, G. *et al.* Carbonyl sulfide (COS) as a tracer for canopy photosynthesis, transpiration and stomatal conductance: potential and limitations. *Plant Cell Environ.* **35,** 657–667 (2012).
11. Hilton, T. W. *et al.* Large variability in ecosystem models explains uncertainty in a critical parameter for quantifying GPP with carbonyl sulphide. *Tellus B Chem. Phys. Meterol.* http://dx.doi.org/10.3402/tellusb.v67.26329 (2015).
12. Commane, R. *et al.* Seasonal fluxes of carbonyl sulfide in a midlatitude forest. *Proc. Natl Acad. Sci. USA* **112,** 14162–14167 (2015).
13. Maseyk, K. *et al.* Sources and sinks of carbonyl sulfide in an agricultural field in the Southern Great Plains. *Proc. Natl Acad. Sci. USA* **111,** 9064–9069 (2014).
14. Whelan, M. E. *et al.* Carbonyl sulfide exchange in soils for better estimates of ecosystem carbon uptake. *Atmos. Chem. Phys.* **16,** 3711–3726 (2016).
15. Campbell, J. E. *et al.* Photosynthetic control of atmospheric carbonyl sulfide during the growing season. *Science* **322,** 1085–1088 (2008).
16. Montzka, S. A. *et al.* On the global distribution, seasonality, and budget of atmospheric carbonyl sulfide (COS) and some similarities to CO_2. *J. Geophys. Res.* **112,** D09302 (2007).
17. Berry, J. *et al.* A coupled model of the global cycles of carbonyl sulfide and CO_2: a possible new window on the carbon cycle. *J. Geophys. Res. Biogeosci.* **118,** 842–852 (2013).
18. Campbell, J. E. *et al.* Atmospheric carbonyl sulfide sources from anthropogenic activity: implications for carbon cycle constraints. *Geophys. Res. Lett.* **42,** 3004–3010 (2015).
19. Andreae, M. O. & Barnard, W. R. The marine chemistry of dimethylsulfide. *Mar. Chem.* **14,** 267–279 (1984).
20. Andreae, M. O. & Ferek, R. J. Photochemical production of carbonyl sulfide in seawater and its emission to the atmosphere. *Glob. Biogeochem. Cycles* **6,** 175–183 (1992).
21. Launois, T., Belviso, S., Bopp, L., Fichot, C. & Peylin, P. A new model for the global biogeochemical cycle of carbonyl sulfide–Part 1: assessment of direct marine emissions with an oceanic general circulation and biogeochemistry model. *Atmos. Chem. Phys.* **15,** 2295–2312 (2015).
22. Aydin, M. *et al.* Changes in atmospheric carbonyl sulfide over the last 54,000 years inferred from measurements in Antarctic ice cores. *J. Geophys. Res. Atmos.* **121,** 1943–1954 (2016).
23. Mahieu, E. *et al.* Observed trends in total vertical column abundances of atmospheric gases from IR solar spectra recorded at the Jungfraujoch. *J. Atmos. Chem.* **28,** 227–243 (1997).
24. Rinsland, C. P. *et al.* Measurements of long-term changes in atmospheric OCS (carbonyl sulfide) from infrared solar observations. *J. Quant. Spectrosc. Radiat. Transf.* **109,** 2679–2686 (2008).
25. Lejeune, B. *et al.* Optimized approach to retrieve information on atmospheric carbonyl sulfide (OCS) above the Jungfraujoch station and change in its abundance since 1995. *J. Quant. Spectrosc. Radiat. Transf.* **186,** 81–95 (2017).
26. Welp, L. R. *et al.* Interannual variability in the oxygen isotopes of atmospheric CO2 driven by El Nino. *Nature* **477,** 579–582 (2011).
27. Beer, C. *et al.* Terrestrial gross carbon dioxide uptake: global distribution and covariation with climate. *Science* **329,** 834–838 (2010).
28. Zhu, Z. *et al.* Greening of the Earth and its drivers. *Nat. Clim. Chang.* **6,** 791–795 (2016).
29. Kolby Smith, W. *et al.* Large divergence of satellite and Earth system model estimates of global terrestrial CO_2 fertilization. *Nat. Clim. Chang.* **6,** 306–310 (2016).
30. Hansen, J., Kharecha, P. & Sato, M. Climate forcing growth rates: doubling down on our Faustian bargain. *Environ. Res. Lett.* **8,** 011006 (2013).
31. Drake, J. E. *et al.* Increases in the flux of carbon belowground stimulate nitrogen uptake and sustain the long-term enhancement of forest productivity under elevated CO_2. *Ecol. Lett.* **14,** 349–357 (2011).
32. Wenzel, S., Cox, P. M., Eyring, V. & Friedlingstein, P. Projected land photosynthesis constrained by changes in the seasonal cycle of atmospheric CO_2. *Nature* **539,** 499–501 (2016).
33. Li, W. *et al.* Reducing uncertainties in decadal variability of the global carbon budget with multiple datasets. *Proc. Natl Acad. Sci. USA* **113,** 13104–13108 (2016).

Supplementary Information is available in the online version of the paper.

Acknowledgements We thank P. Friedlingstein for climate-model data; D. Streets for inventory suggestions; and P. Koch, C. Tebaldi, D. Lobell, P. Peylin, N. Petra, A. Wolf, J. Schnoor and C. Field for comments on our study. This work was supported by the US Department of Energy, Office of Science, Office of Terrestrial Ecosystem Sciences (grant no. DE-SC0011999). S.A.M. acknowledges support in part from the National Oceanic and Atmospheric Administration (NOAA) Climate Program Office's AC4 program, and the firn-modelling expertise of M. Battle and M. Aydin. M.L. was supported by the Academy of Finland as part of the INQUIRE project (grant no. 267442). L.B. acknowledges support from H2020 project CRESCENDO (grant 641816). T.L. was supported by the European Research Council (ERC) early career starting grant SOLCA (grant no. 338264).

Author Contributions J.E.C. and J.A.B. designed the research. J.E.C. conducted all simulations and analysis, except ocean simulations, which were run by L.B., T.L. and S.B., Markov chain Monte Carlo scenarios, which were run by M.L., and relative uptake simulations, which were run by U.S. J.E.C. wrote the paper with input from all co-authors.

Author Information Reprints and permissions information is available at www.nature.com/reprints. The authors declare no competing financial interests. Readers are welcome to comment on the online version of the paper. Publisher's note: Springer Nature remains neutral with regard to jurisdictional claims in published maps and institutional affiliations. Correspondence and requests for materials should be addressed to J.E.C. (ecampbell3@ucmerced.edu).

Reviewer Information *Nature* thanks P. Friedlingstein, N. Gruber, D. Yakir and the other anonymous reviewer(s) for their contribution to the peer review of this work.